

1 Drainage of high-consistency fiber-laden aqueous foams

2 Antti Koponen, Oleg Timofeev, Ari Jäsberg, and Harri Kiiskinen

3 *VTT Technical Research Centre of Finland*

4 Correspondence:

5 Antti Koponen

6 VTT Technical Research Centre of Finland, P.O. Box 1603, FIN-40401 Jyväskylä, Finland

7 Tel. +358 20 722 2717

8 Fax. +358 20 722 2596

9 Email: Antti.Koponen@vtt.fi

10 Keywords: fiber-laden foam, foam forming, drying, drainage, lightweight cellulose materials,
11 lightweight fibrous structures

12 **Abstract**

13 Lightweight lignocellulosic fibrous materials (LLFMs) offer a sustainable and biodegradable
14 alternative in many applications. Enthusiastic interest in these materials has recently grown together
15 with the newly risen interest in foam forming. Foam bubbles restrain fiber flocculation, and foam
16 formed structures have high uniformity. Moreover, the bubbles support the fibrous structure during
17 manufacturing enabling the formation of highly porous structures. Mechanical pressure cannot be
18 applied in the manufacture of LLFMs as the materials would lose their porous structure. Water is
19 therefore typically removed by a combination of drainage and thermal drying. Thermal drying of
20 porous materials has been studied intensively. However, there are only a few studies on the drainage
21 of fiber-laden foams. Thus, in this work, we conducted a systematic analysis of this topic. Our
22 findings show that after drainage a stationary horizontal moisture profile similar to that of pure foams
23 is developed. Raising the initial fiber consistency was found to increase the final fiber consistency of
24 the foam until the drainage ceased. Increasing mold height was found to increase the final consistency
25 considerably. Without vacuum and heating, the shrinkage of samples during drainage was only
26 slightly higher than the volume of the drained water. Drainage rate and final consistency increased
27 clearly with increasing vacuum, but simultaneously sample shrinkage increased considerably. The
28 best compromise was obtained with a vacuum of 0.5 kPa, which increased the final consistency by

29 60% without extra shrinkage. Using warm foam and heating the foam during drainage increased the
30 final consistency considerably, but this also led to significant shrinkage of the sample.

31

32 **Introduction**

33 Lightweight lignocellulosic fibrous materials (LLFMs) offer a sustainable and biodegradable
34 alternative in many applications such as thermal insulation (Pöhler, Jetsu, Fougerón, & Barraud,
35 2017), sound insulation (Nechita & Năstac, 2018; Debeleac, Nechita, & Nastac, 2019), interior
36 decoration (Härkäsalmi et al., 2017; Siljander et al., 2019), polymer-impregnated composites, and
37 packaging (Satyanarayana, Arizaga, & Wypych, 2009; Huber et al., 2012). As lignocellulosic fibers
38 have strong aggregation tendency, LLFMs are difficult to produce with conventional water forming.
39 However, due to the recent resurgence of foam forming, interest in these materials is now growing
40 rapidly.

41 In foam forming, fibers are mixed with water and surfactants to create a fiber-laden foam with a
42 typical air content of 50-70% (Punton, 1975b, 1975a; Smith & Punton, 1975; Smith, Punton, &
43 Rixson, 1974; Poranen et al., 2013; Koponen, Torvinen, Jäsberg, & Kiiskinen, 2016; Lehmonen,
44 Retulainen, Paltakari, Kinnunen-Raudaskoski, & Koponen, 2020). The bubbles restrain flocculation
45 in the foam, and the formed structures obtain much better uniformity than achieved with water.
46 Moreover, the bubbles support the fibrous structure during manufacturing, enabling the production
47 of highly porous structures with densities lower than 10 kg/m³ (Korehei, Jahangiri, Nikbakht,
48 Martinez, & Olson, 2016; Burke, Möbius, Hjelt, & Hutzler, 2019). Finally, much higher consistencies
49 can be used with foam when compared to water, which gives improved energy and water efficiency.

50 When making LLFMs with aqueous foams, water is usually removed from the fibrous structures in
51 two steps. The first step is dewatering (drainage), in which water flows in the fiber-laden foam
52 downwards due to gravity and is removed at the bottom of the sample. After drainage, the capillary
53 pressure and gravity are in balance and the foam has a stationary moisture profile. The second step is
54 thermal drying, in which the remaining water is removed from the structure by evaporation.
55 Mechanical pressure cannot be used in either step as the samples would lose their porous structure.
56 However, low vacuum can be used to speed up the process and make it more efficient. Porous
57 cellulosic structures can also be produced with other methods, such as freeze-drying (Nicholas
58 Tchang Cervin, Aulin, Larsson, & Wågberg, 2012; Korehei et al., 2016; Josset et al., 2017),
59 supercritical carbon dioxide drying (Sehaqui, Zhou, Ikkala, & Berglund, 2011) and air-drying from

60 volatile organic solvents (Wege, Kim, Paunov, Zhong, & Velev, 2008). However, these methods are
61 hardly viable for commercial low-cost large-scale production of LLFMs.

62 Thermal drying of porous structures is a technological problem that has been studied intensively
63 (Kowalski, 2007; Xu, Sasmito, & Mujumdar, 2019). Considerable knowledge has been gained on
64 thermal drying of foam-like materials in the food industry (Hertzendorf, Moshy, & Seltzer, 1970;
65 Kudra & Ratti, 2006; Sangamithra, Venkatachalam, John, & Kuppaswamy, 2015) and thermal drying
66 of fibrous structures in the paper industry (Stenström, 2019) and nonwoven industry (Lyons &
67 Vollers, 1971). Although LLFMs are novel materials, there are already a few studies dedicated to
68 their thermal drying. Thermal drying of LLFMs has been studied at room temperature by Korehei et
69 al. (2016), Nechita and Năstac (2018), and Burke et al. (2019), and at higher temperatures by
70 Alimadadi and Uesaka (2016), Pöhler et al. (2017), and Härkäsalmi et al. (2017). Moreover,
71 Timofeev, Jetsu, Kiiskinen, & Keränen (2016) have studied thermal drying of LLMFs with infrared
72 heating in combination with vacuum and impingement drying (hot air jet).

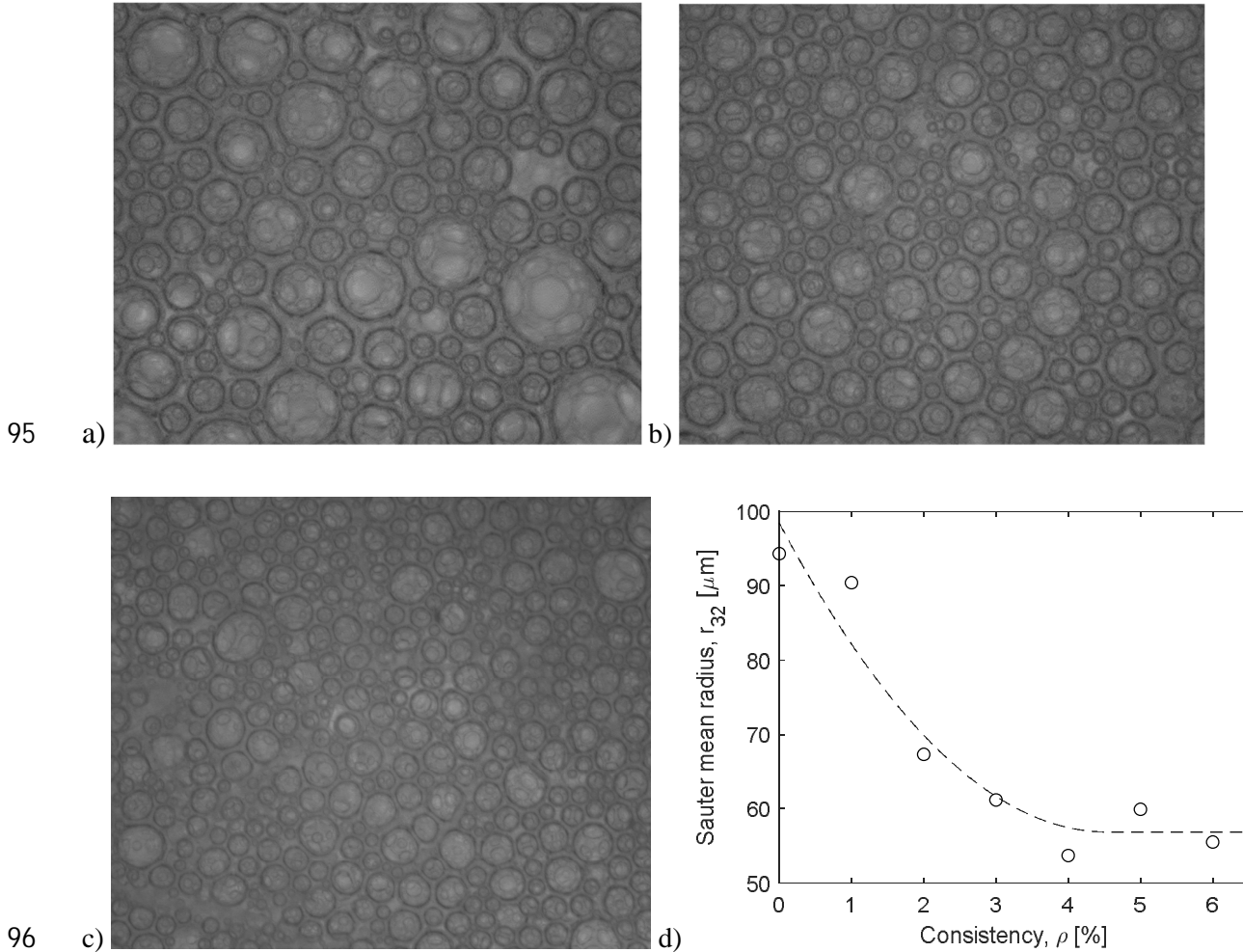
73 The drainage process of pure foams has been studied extensively (Verbist, Weaire, & Kraynik, 1996;
74 Koehler, Hilgenfeldt, & Stone, 2000; Saint-Jalmes, 2006; Stevenson, 2006; Kruglyakov, Karakashev,
75 Nguyen, & Vilkova, 2008; Papara, Zabulis, & Karapantsios, 2009; Kruglyakov, Elaneva, Vilkova, &
76 Karakashev, 2010; Arjmandi-Tash, Kovalchuk, Trybala, & Starov, 2015; Koursari, Arjmandi-Tash,
77 Johnson, Trybala, & Starov, 2019; Koursari et al., 2019). However, there are few studies on the
78 drainage of fiber-laden foams (Haffner, Dunne, Burke, & Hutzler, 2017).
79 Analysis of the drainage of fiber-laden foams is therefore relevant from both a practical and academic
80 point of view. There is also a lack of studies of the effect of vacuum on the drainage of fiber-laden
81 foams (Korehei et al., 2016). Such studies, however, have significant practical relevance for
82 optimization of the dewatering phase to save both time and energy during thermal drying.

83 In this work, we systematically analyze the drainage of fiber-laden foams. We study the effect of
84 initial fiber consistency, fiber type and mold height on the final consistency and shrinkage of fiber-
85 laden foams. In addition, we analyze the effect of vacuum and heating on drainage and shrinkage.

86 **Materials and methods**

87 Three pulps were used as the raw material for the fibrous samples: virgin pine fiber, virgin birch fiber,
88 and chemi-thermomechanical pulp (CTMP, CSF 600). In the experiments, the fiber consistency was
89 varied from 2% to 8%. Sodium dodecyl sulfate (SDS, purity at least 90%) surfactant was used as the
90 foaming agent.

91 The foams were made at room temperature ($T \sim 18 - 22$ °C) from tap water with an SDS dosage of
 92 0.6 g/l. The surface tension was $\sigma \approx 35$ mN/m (Lehmonen et al., 2020). The effect of SDS on
 93 viscosity is rather small. At an SDS dosage of 4 g/l, the viscosity of the SDS solution is less than 4%
 94 higher than pure water, which is at 20 °C 1.0 mPas (Kushner, Duncan, & Hoffman, 1952).



97 **Figure 1** Microscopic images (1.7 mm \times 2.0 mm) of aqueous foam samples taken from the mixing
 98 tank: a) Pure foam. b) Fiber consistency 2.0%. c) Fiber consistency 6.0%. d) Sauter mean radius of
 99 bubbles as a function of consistency. Dashed line is a visual guide.

100 The foams were produced by mixing the fiber suspension and surfactant with air in a tank (tank
 101 diameter 125 mm, height 430 mm). A circular disc with a diameter of 83 mm and two opposing 25
 102 degree bends was used as the mixing blade. Mixing was improved by moving the impeller up and
 103 down during mixing. Mixing speed was 3500 rpm and mixing time was 15 min. The air fraction of
 104 the produced foam was 65-70%.

105 The Sauter mean diameter of foam bubbles is defined as

106

$$r_{32} = \frac{\sum_{i=1}^n f_i r_i^3}{\sum_{i=1}^n f_i r_i^2}, \quad (1)$$

107 where f_i and r_i are, respectively, the number and radius of bubbles in a particular size fraction i . Sauter
 108 mean radius reflects the size of identical spherical bubbles, a system of which has the same total
 109 surface area and total volume as a system of multisized bubbles (Kowalczyk & Drzymala, 2016). The
 110 total surface energy of the monosized bubbles is then equal to the total surface energy of polysized
 111 bubbles. As surface energy is a fundamental quantity for foams, Sauter mean radius is widely used
 112 for describing the mean size of bubbles. Figure 1 shows the Sauter mean radius of bubbles as a
 113 function of consistency. Bubble size was measured using the method presented by Lappalainen and
 114 Lehmonen (2012). We can see in Figure 1 that bubble radius reaches equilibrium with increasing
 115 consistency, being ca. 55 - 60 μm when the consistency exceeds 4%.

116



117

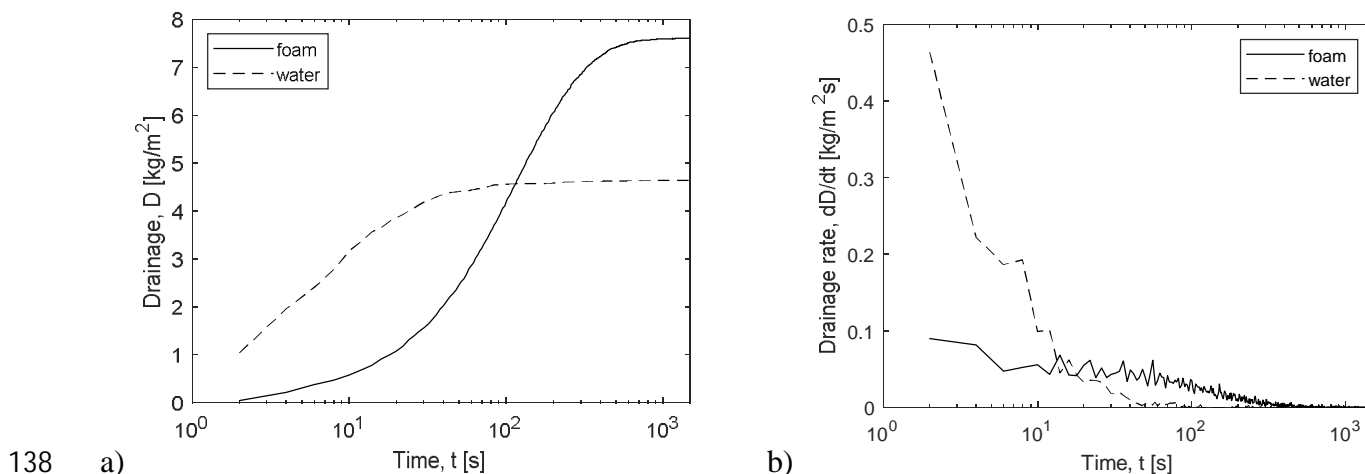


118 **Figure 2** a) Examples of used molds. Height from left to right: 15 mm, 25 mm and 40 mm. Inner
 119 diameter 165 mm. b) Examples of final drained and dried samples made with the above molds.

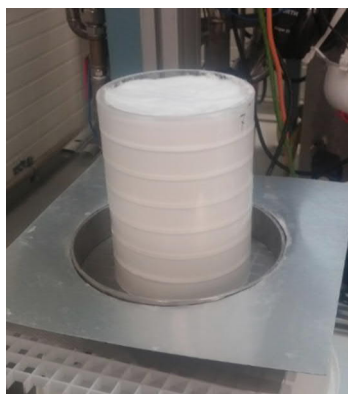
120 After mixing, the foam was poured into cylindrical molds with an inner diameter of 165 mm. The
 121 height of the single-ring molds varied from 10 mm to 100 mm (for examples see Figure 2a). Using
 122 molds with different heights made it possible to analyze the drainage process with different sample
 123 thicknesses (see Figure 2b). Drainage time was in most cases ca. 25 minutes. A metal screen (stainless
 124 steel mesh) in the bottom of the molds retained the fibers while allowing the water to run out of the
 125 molds with low resistance. The water runoff was collected and its mass was recorded at 0.5 Hz
 126 frequency using a digital laboratory balance. In some cases, the time evolution of the thickness of the

127 samples was also recorded with laser line profiling using a frequency of 2.5 Hz. Notice that this setup
128 cannot be used for analyzing the drainage of pure foams, as pure foams pass through the metal screen.

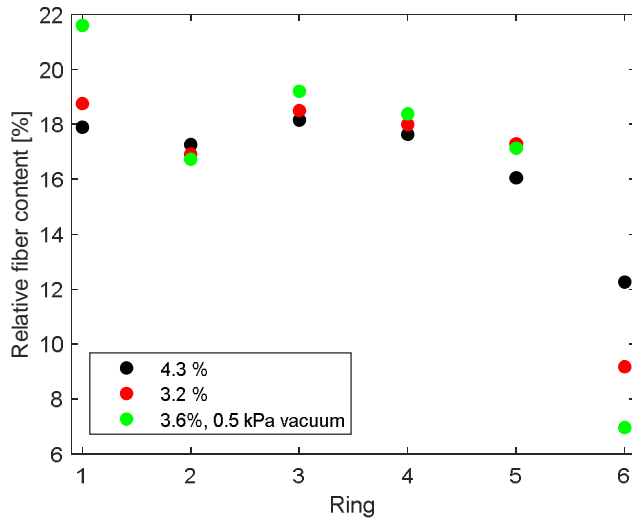
129 Figure 3 shows a comparison of drainage and drainage rate of a fiber-laden foam (air content 70%)
130 and a water-fiber suspension as a function of time for CTMP pulp in a 40 mm mold. In both cases the
131 initial consistency (fiber mass divided by the combined mass of water and fibers) is 3% and the
132 amount of water is the same. Foam and water are seen to behave very differently. The drainage rate
133 of water is initially very high (five times that of foam) but it decreases rapidly. As a result, the samples
134 made with foam have a much higher final consistency even though the initial consistencies are equal.
135 Foam forming has great potential for the manufacture of porous fiber-based products; not only due to
136 the ability to make low-density uniform structures, but also due to improving the dryness of the
137 produced (wet) fibrous samples.



139 **Figure 3** Comparison of a) drainage (mass of drained water per unit area) and b) drainage rate of a
140 fiber-laden foam and a fiber-water suspension as a function of time. Consistency of the CTMP fiber
141 is 3% and the mold height is 40 mm. Final consistency is 7.0% for foam and 4.5% for water.



143 **Figure 4** Seven-ring mold used for vertical consistency analysis. Mold height 140 mm.



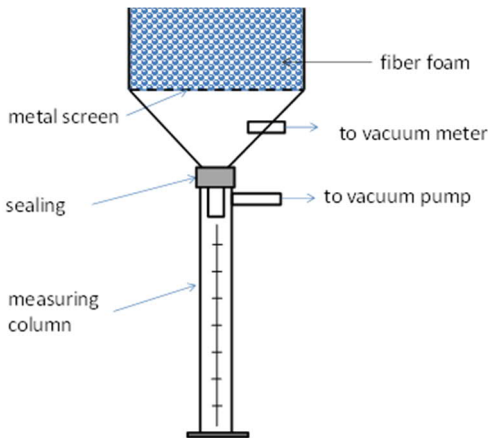
144

145 **Figure 5** Relative fiber content per ring (sum of all rings is 100%) in the seven-ring mold after
 146 drainage with and without low vacuum. 1 = bottom ring, 6 = ring below the top ring. The sample
 147 compressed during drainage; thus ring 7 was empty and ring 6 only partly filled. Some experimental
 148 variations in relative consistencies were present, but free drainage does not seem to create a significant
 149 height-dependent fiber density profile in the sample. With low vacuum, relative consistency is slightly
 150 higher in the bottom ring compared to the other rings.

151 A seven-ring mold with a height of 140 mm was used to analyze the vertical consistency profile of
 152 the sample after drainage (see Figure 4). Ring height was 20 mm and inner diameter 100 mm. The
 153 mold was filled to the brim with fiber foam, and drainage was completed in 35 minutes. After
 154 drainage, each ring was removed separately, and the fiber-foam was skimmed from the mold with a
 155 thin metal plate onto aluminum plates. The wet fiber-foam samples were weighed, dried in an oven
 156 at 105 °C, and then reweighed. Three measurements were performed with pine fiber with initial
 157 consistencies of 4.3%, 3.2% and 3.6% (the last with 0.5 kPa vacuum). During drainage the sample
 158 shrank in the seven-ring mold by approximately 30 mm; by the end the top ring was empty and only
 159 50-75% of the following ring was filled with fiber-foam (see Figure 5). The fiber content of the other
 160 rings was approximately equal. Free drainage thus did not seem to create a significant height-
 161 dependent fiber density profile in the sample. When a low vacuum was used the number of fibers was
 162 slightly higher in the bottom ring compared to the other rings. Note that Burke et al. (2019) observed
 163 at the sample top and bottom a ca. 3 mm layer of higher fiber concentration. We did not examine this
 164 in our study, but our samples are assumed to have a similar structure. It is also noteworthy that, unlike
 165 our study and that of Burke et al. (2019), Haffner et al. (2017) studied the liquid drainage using a
 166 closed mold, which resulted in a sharp downward gradient of fiber concentration. The reason for this
 167 behavior is unclear.

168 Drainage can be accelerated by increasing the temperature of the fiber-laden foam or by using a
169 vacuum. Increased temperature reduces water viscosity. As a result, the water flow resistance of the
170 fiber-foam structure is lowered, enabling water to flow more easily through it. Further improvement
171 of drainage can be achieved by creating an upward temperature gradient across the foam. The
172 resulting thermocapillary Marangoni effect creates a surface tension gradient that accelerates the
173 downward flow of water (Miralles, Selva, Cantat, & Jullien, 2014).

174 The effect of vacuum, foam temperature and heating on drainage was studied with the setup shown
175 in Figure 6. The measurement device comprised a mold fitted with a metal screen at the bottom, a
176 measuring column, and a rubber seal. The measuring column was connected to a vacuum pump, and
177 vacuum under the sample mold was measured. The amount of drained liquid was measured with a
178 ruler. Foam temperature was measured using a K-type thermocouple located at the bottom of the
179 sample mold. In some cases, the fiber mass was first heated to 50-55 °C and then foamed. The warm
180 fiber foam was then poured into the sample mold. Cooling of the heated foam could be slowed during
181 drainage using an infra heater installed above the sample mold (this also created an upward
182 temperature gradient in the foam). In these tests, pine fiber was used at 2.0% initial consistency. The
183 mold height was 80 mm.



184

185 **Figure 6** Schematic of the mold with vacuum at the bottom.

186

187

188

189 **Table 1** Trial points of the drainage experiments with variable initial consistency. Left to right: trial
 190 point, furnish, mold height (H_m), initial consistency (ρ_i), final consistency (ρ_f), amount of water
 191 removed (w), total sample height shrinkage (Δh), sample height shrinkage due to air leakage (Δh_{air}),
 192 and initial air content (φ).

TP	Furnish	H_m [mm]	ρ_i [%]	ρ_f [%]	w [%]	Δh [%]	Δh_{air} [%]	φ [%]
1	CTMP	40	2.9	7.0	61	23.8	2.7	65
2	CTMP	40	3.0	6.5	55	24.8	7.3	66
3	CTMP	40	3.2	6.8	55	-	-	-
4	CTMP	40	3.7	7.0	50	19.6	4.4	69
5	CTMP	40	5.0	7.6	36	-	-	-
6	CTMP	40	5.1	7.3	32	16.5	7.1	70
7	CTMP	40	5.7	7.4	24	13.1	6.4	71
8	CTMP	40	6.8	7.7	13	8.5	4.7	70
9	CTMP	40	7.0	8.0	13	9.3	5.4	70
10	CTMP	40	7.5	8.1	8	6.7	4.1	68

193

194 **Results**

195 *Effect of initial consistency on drainage*

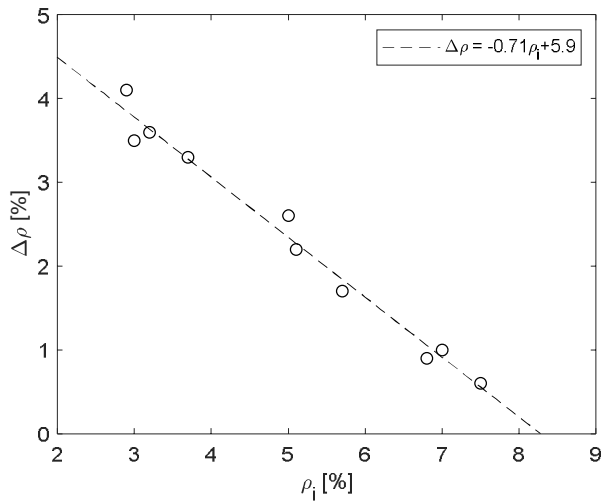
196 The effect of initial consistency on drainage was studied with CTMP furnish in a 40 mm mold. Table
 197 1 shows for these trial points the initial height of the sample i.e. mold height, H_m , the initial
 198 consistency, ρ_i , final consistency, ρ_f , the amount of water removed, w , the total shrinkage of the
 199 sample height, Δh , the shrinkage of the sample height due to the leakage of air, Δh_{air} , and the initial
 200 air content, φ . Initial air content was calculated using the formula:
 201

$$202 \quad \varphi = 1 - \left[(m_{\text{wet}} + m_d - m_{\text{dry}}) / \rho_w + m_{\text{dry}} / \rho_p \right] / Ah_i, \quad (2)$$

203 where A is the cross sectional area of the mold, h_i is the initial height of the sample, m_{wet} is the mass
 204 of the wet sample after drainage, m_d is the mass of drained water, m_{dry} is the mass of the sample after
 205 drying, $\rho_w = 1000 \text{ kg/m}^3$ is the density of water, and $\rho_p = 1500 \text{ kg/m}^3$ is the density of pulp fiber.
 206 Shrinkage of the sample height due do air leakage was calculated from $\Delta h_{\text{air}} = \Delta h - m_d / A\rho_w$.

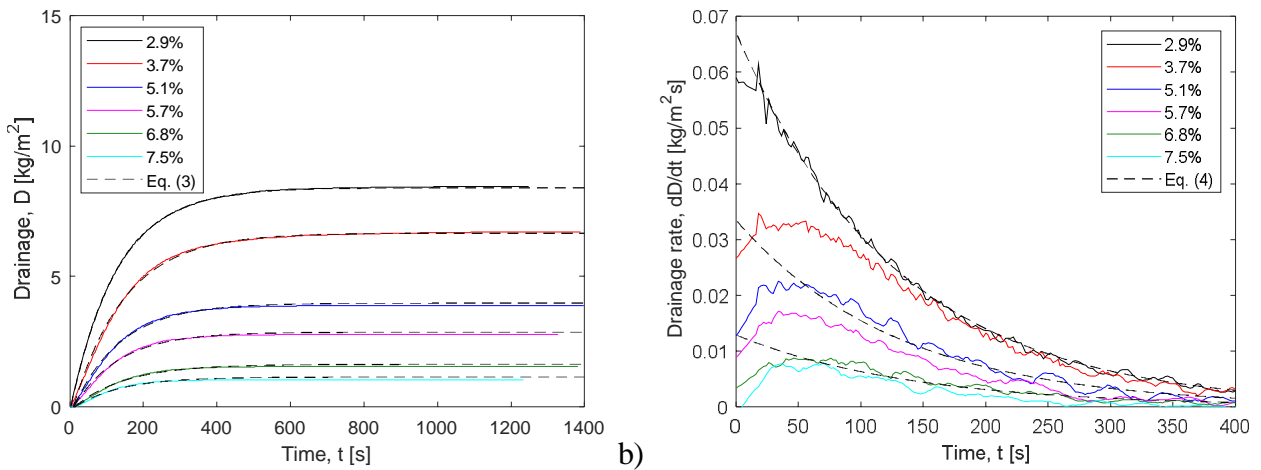
207 We can see from Table 1 that final consistency increases gradually with increasing initial consistency.
 208 Figure 7 shows the consistency change $\Delta\rho = \rho_f - \rho_i$ as a function of initial consistency ρ_i . The dashed
 209 line shows a linear fit $\Delta\rho = -0.71\rho_i + 5.9$ with the data points. When $\Delta\rho = 0$, this formula gives

210 $\rho_i = 8.3\%$. It is likely that with higher initial consistencies drainage would be negligible with this mold
 211 height.



212

213 **Figure 7** Consistency change $\Delta\rho = \rho_f - \rho_i$ as a function of initial consistency ρ_i .



214

215 **Figure 8** a) Drainage, b) drainage rate as a function of time for CTMP pulp with various initial
 216 consistencies. The dashed lines in a) and b) are the fits of Eqs. (3) and (4) to the measured drainage
 217 and drainage rate curves, respectively. Mold height 40 mm.

218 Figure 8 shows the drainage and drainage rate as a function of time for various consistencies. Note
 219 that, due to experimental noise, the drainage rate curves have been obtained by filtering the original
 220 data with Matlab's smooth function using a Savitzky–Golay filter with a 20-point window. We can
 221 see from Figure 8b that initially there is a short transient phase of ca. 20 seconds during which the
 222 drainage rate increases. After that, the drainage rate decreases monotonically.

223 After the initial transient phase, ending at time t_0 , drainage follows very accurately with all
 224 consistencies the formula ($R^2 > 0.98$, see dashed lines in Figure 8a):

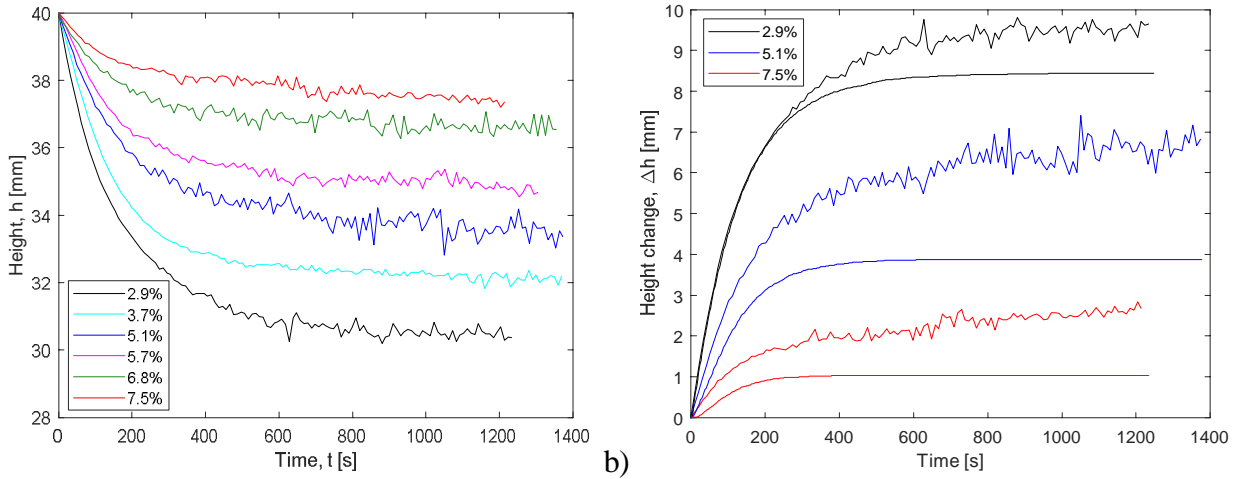
225
$$D = M \left(1 - e^{-(t-t_0)/T} \right), t > t_0. \quad (3)$$

226 Parameter T , which gives the time scale of the drainage process, is approximately equal, $T \approx 130$ s, in
 227 all cases. The dynamics of the drainage process is thus independent of the initial consistency. Notice
 228 that Eq. (3) gives as the drainage rate

229
$$\frac{dD}{dt} = \frac{M}{T} e^{-(t-t_0)/T}, t > t_0. \quad (4)$$

230 Drainage rate thus decreases exponentially as a function of time. We can see from Figure 8b that Eq.
 231 (4) works well after the initial transient phase.

232



233 a) b)
 234 **Figure 9** a) Sample height as a function of time for various initial consistencies of CTMP pulp. Mold
 235 height 40 mm. Initial sample height varied from 40-43 mm. The profiles are normalized to start at h
 236 = 40.0 mm to facilitate reading the graph. b) Measured change in sample height (fluctuating lines)
 237 and height change calculated from drained water (smooth lines).

238 *Compression during drainage*

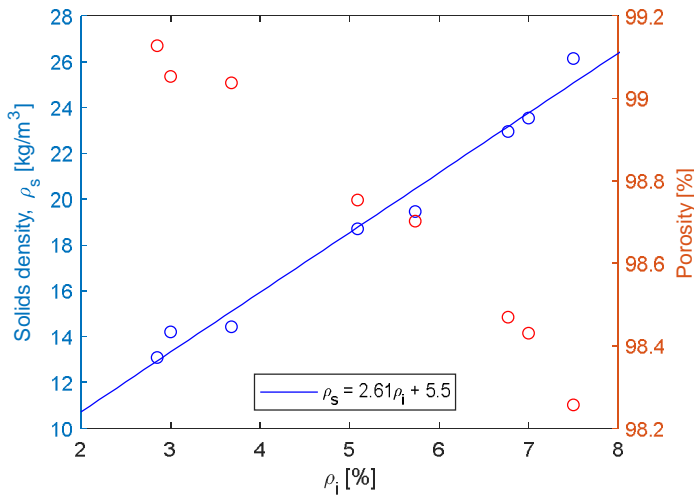
239 As Table 1 shows, the fiber foam samples compressed during drainage. With highest initial
 240 consistencies sample compression is less than 10%, while with lowest consistencies compression is
 241 up to 25%. Figure 9a shows the time development of sample thickness during drainage. Figure 9b
 242 compares the change in sample height with that calculated from the volume of drained water. We can
 243 see from Figure 9b that the sample compression is due to both water draining and leakage of air. The
 244 decrease in sample height due to air leakage varies between 3-7%, and no systematic dependence on

245 initial consistency is seen. Most bubbles thus seem to remain intact during drainage, supporting the
 246 fibrous structure and preventing its collapse.

247 For the trial points shown in Table 1, compression is linearly dependent on initial consistency ($R^2 =$
 248 0.98):

$$249 \quad \Delta h_{\%} = -3.75\rho_i + 34.8\%. \quad (5)$$

250 (Above ρ_i and $\Delta h_{\%}$ are expressed in percentages.) Notice that Eq. (5) is closely in line with the
 251 shrinkage observed for pine fibers when the 7-ring mold was used. As we did not always perform
 252 height measurement during drainage, we used Eq. (5) below in some cases to estimate the final sample
 253 height after drainage.



254
 255 **Figure 10** Solids density and porosity of the final CTMP samples as a function of initial consistency,
 256 with the assumption that all residual water has been removed without changing the sample structure.
 257 Mold height 40 mm.

258 The height measurement data can be used for analyzing the geometrical properties of the structure of
 259 the final sample. Figure 10 shows the solids density, ρ_s , and porosity of the final drained samples
 260 before drying when the remaining water is omitted from the analysis. (We have, i.e., assumed that all
 261 residual water has been removed without changing the 3D structure of the sample.) We see from
 262 Figure 10 that the samples are very porous before drying and solids density is a linear function of
 263 initial density

$$264 \quad \rho_s = 2.61\rho_i + 5.5. \quad (6)$$

265
 266 Above, ρ_i is expressed in percentages and ρ_s in kg/m^3 . Note that by extrapolating Eq. (6) to very dilute
 267 initial consistencies ($\rho_i \rightarrow 0$), one gets $\rho_s = 5.5 \text{ kg/m}^3$. This is close to the density of pine fiber

268 networks, $\rho_s = 4 \text{ kg/m}^3$, obtained with foam forming and freeze drying with 0.5% initial consistency
 269 and a 20 mm mold (Korehei et al., 2016). Burke et al. (2019) used pine fiber with a 50 mm mold and
 270 dried the samples for 40 hours at room temperature. With an air content of 67% and initial fiber
 271 density of 1.0%, the solids density of the dry samples was 8.8 kg/m^3 , which is well in line with Eq.
 272 (6).

273 **Table 2** Drainage experiments conducted with mold heights of 10-100 mm. Initial consistency was
 274 kept constant, but in practice varied between 3.1-3.8%. Left to right: trial point, furnish, mold height,
 275 initial consistency, final consistency, and amount of removed water. Note that trial points 28-30 are
 276 averages over two measurements.

TP	Furnish	H_m [mm]	ρ_i [%]	ρ_f [%]	w [%]
11	pine	10	3.3	4.5	28
12	pine	20	3.4	6.2	46
13	pine	30	3.5	6.9	51
14	pine	40	3.4	7.8	58
15	pine	60	3.1	8.3	65
16	pine	80	3.2	9.3	68
17	pine	100	3.2	10.0	70
18	birch	10	3.6	4.4	19
19	birch	20	3.6	5.2	31
20	birch	30	3.7	5.9	38
21	birch	40	3.5	6.1	44
22	birch	60	3.5	7.0	51
23	birch	80	3.6	7.8	56
24	birch	100	3.7	8.3	57
25	CTMP	10	3.4	5.1	34
26	CTMP	20	3.8	4.8	23
27	CTMP	30	2.8	4.6	41
28	CTMP	40	3.3	6.1	47
29	CTMP	60	3.1	7.3	58
30	CTMP	80	3.3	8.0	61
31	CTMP	100	3.3	8.8	64

277

278 *Effect of mold height on final consistency*

279 Table 2 shows the furnish, mold height, initial consistency, final consistency, and the amount of
 280 removed water, for the drainage experiments made with mold heights of 10-100 mm. Consistency
 281 was approximately constant, varying between 3.1% and 3.8% and averaging at 3.4%. A linear
 282 regression analysis of the data shown in Table 1 gives for final consistency ($R^2 = 0.98$)

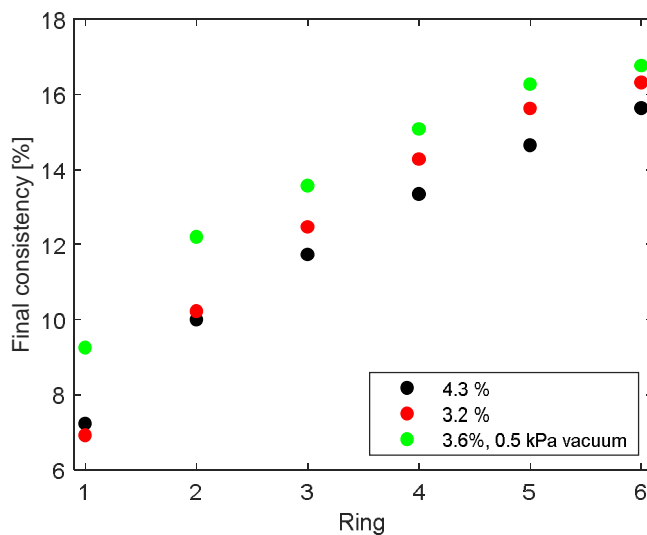
283

$$\rho_f = 5.6 + 0.044H_m + \beta, \quad (7)$$

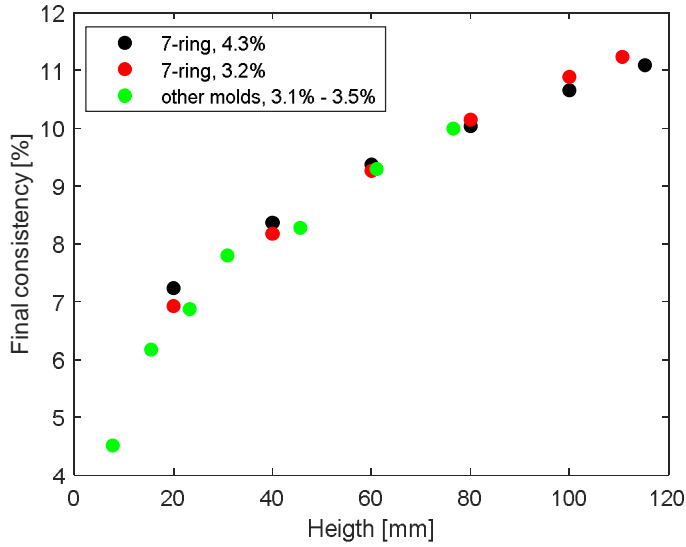
284 where β is a classifying parameter which is zero for pine, -1.4 for birch, and -1.2 for CTMP.
 285 Consistency is expressed in Eq. (7) in percentages and mold height in millimeters. Note that trial
 286 points 11 and 27 were outliers and were omitted from the regression analysis. For other trial
 287 Eq. (1) works very well, and the relative difference between the modelled final consistency and the
 288 measured final consistency is always less than 0.1. On average, the relative difference is only 0.03.

289 We see from Eq. (7) that final consistency increases with increasing mold height. As we see below,
 290 this can be explained by a consistency profile that is developed during drainage. Pine has a more than
 291 one percentage point higher final consistency than birch and CTMP. This is probably due to pine
 292 fibers having larger diameter and smaller specific surface area than birch and CTMP fibers. Thus, the
 293 average pore size of pine samples is probably bigger (this decreases the capillary pressure) and the
 294 available wetting surface is smaller (there is less room for water to be absorbed) than for birch and
 295 CTMP.

296 Figure 11 shows the consistency in each ring of the seven-ring mold. We see that there is a vertical
 297 consistency profile in the samples. Consistency increases monotonically from bottom to top and the
 298 profiles for the two non-vacuum measurements are very similar. When a low vacuum is used,
 299 consistency increases more in the vicinity of sample bottom. At the top the effect of the vacuum is
 300 minimal.



301
 302 **Figure 11** Final consistency in each ring of the seven-ring mold after drainage. 1 = bottom ring, 6 =
 303 ring below the top ring. Consistency increases monotonically from bottom to top. With low vacuum
 304 consistency increases more at the bottom of the sample. Pine fiber was used. Initial consistencies are
 305 given in the legend.



306

307 **Figure 12** Final consistency as a function of sample height. 10-100 mm molds and seven-ring mold
 308 data are shown. Shrinkage differed slightly between the two seven-ring samples, which explains the
 309 slightly different position of the highest data point. Pine fiber was used. Initial consistencies are given
 310 in the legend.

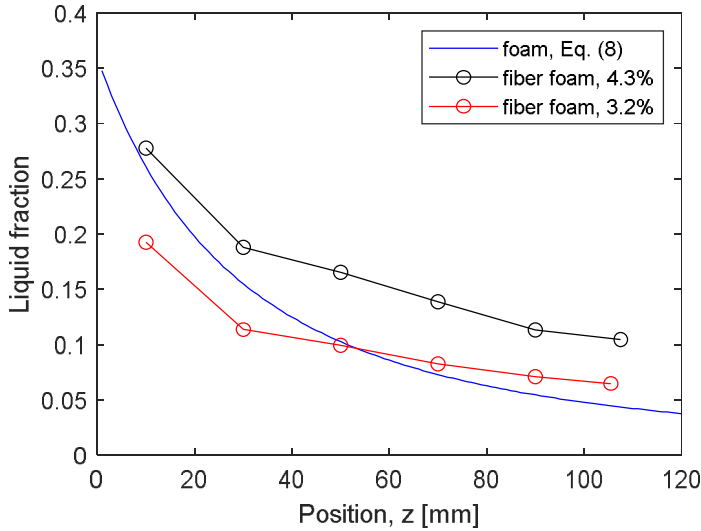
311 Figure 12 shows the final consistency as a function of sample height. The data for 10-100 mm molds
 312 is for pine fiber. The final sample heights for the 10-100 mm molds were obtained from Eq. (5). The
 313 7-ring data presented in Figure 12 is cumulative; the consistency at a given height is an average over
 314 the rings below that point. We can see that the different data sets agree very well with each other.
 315 Final consistency increases systematically with increasing sample height.

316 When pure foam is in contact with the drained water the dependence of volumetric water content
 317 (liquid fraction) on height, z , at the end of the drainage process is obtained from the formula (Haffner
 318 et al., 2017):

$$319 \quad \phi_{\text{eq}}(z) = \left[\frac{1}{\sqrt{\phi_c}} + \sqrt{3} \frac{r_{32}}{\lambda_c^2} z \right]^{-2}, \quad (8)$$

320 where $\phi_c = 0.36$ is the water content below which the foam has a yield stress, r_{32} is the bubble radius,
 321 and $\lambda_c = \sqrt{\sigma/\rho g}$ is the capillary length (here σ is the surface tension, and ρ is the density of water).
 322 When deriving Eq. (8) it is assumed that the bubble size does not change during drainage (no
 323 coarsening or coalescence). While this assumption is an approximation, it is quite reasonable here as
 324 fibers slow down coalescence (Mira et al., 2014; Li et al., 2016).

325 Figure 13 shows with $r_{32} = 60 \mu\text{m}$ (see Figure 1) the liquid fraction as a function of horizontal position,
 326 z , in the sample for a pure foam together with the measured liquid fractions for fiber foams using the
 327 seven-ring mold. The theoretical and experimental profiles are rather similar. In our setup, the
 328 draining fiber foam is not in contact with the drained water. The metal screen, however, may hold
 329 some water in its voids creating an effective water boundary at the bottom of the mold. This may be
 330 one reason for the similarity of the curves shown in Figure 13.



331

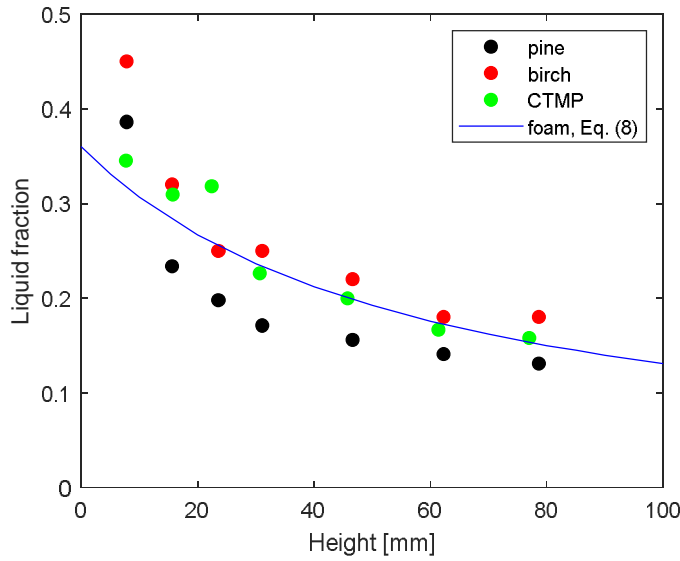
332 **Figure 13** Local liquid fraction as a function of horizontal position after drainage for pure foam
 333 together with the measured liquid fractions for fiber-laden foams. The measurement was performed
 334 with the seven-ring mold using pine fiber.

335 For pure foam that is in contact with water the final liquid fraction after drainage is (Haffner et al.,
 336 2017):

337

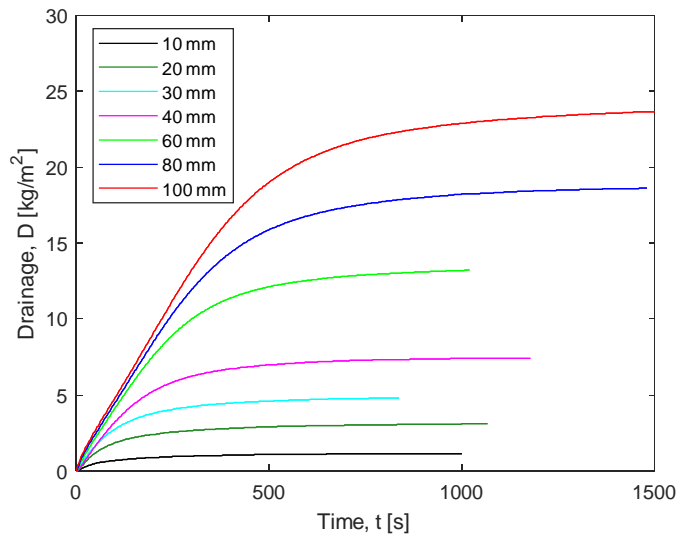
$$\bar{\phi}_{\text{eq}} = \frac{\lambda_c^2 \sqrt{\phi_c}}{\sqrt{3} H r_{32}} \left[1 - \frac{1}{1 + \sqrt{3} H \frac{r_{32}}{\lambda_c^2} \sqrt{\phi_c}} \right], \quad (9)$$

338 where H is the sample height. Figure 14 shows the theoretical liquid fraction together with the
 339 measured results for pine and birch with $r_{32} = 60 \mu\text{m}$. The agreement between the theoretical
 340 prediction for pure foams and the experimental data is quite good.



341

342 **Figure 14** Theoretical liquid fraction (see Eq.(8)) of pure foam and the measured liquid fractions for
 343 fiber foams made with the 10-100 mm molds from pine (initial consistency ca. 3.3%), birch (initial
 344 consistency ca. 3.6%) and CTMP (initial consistency ca. 3.3%) as a function of final sample height
 345 (calculated from Eq. (5)).



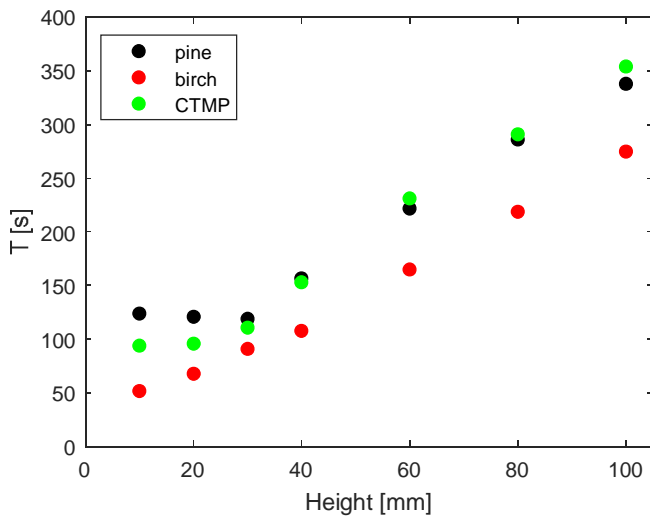
346

347 **Figure 15** Drainage as a function of time for various mold heights for pine. Initial consistency was
 348 on average 3.3%.

349 *Drainage dynamics with different mold heights*

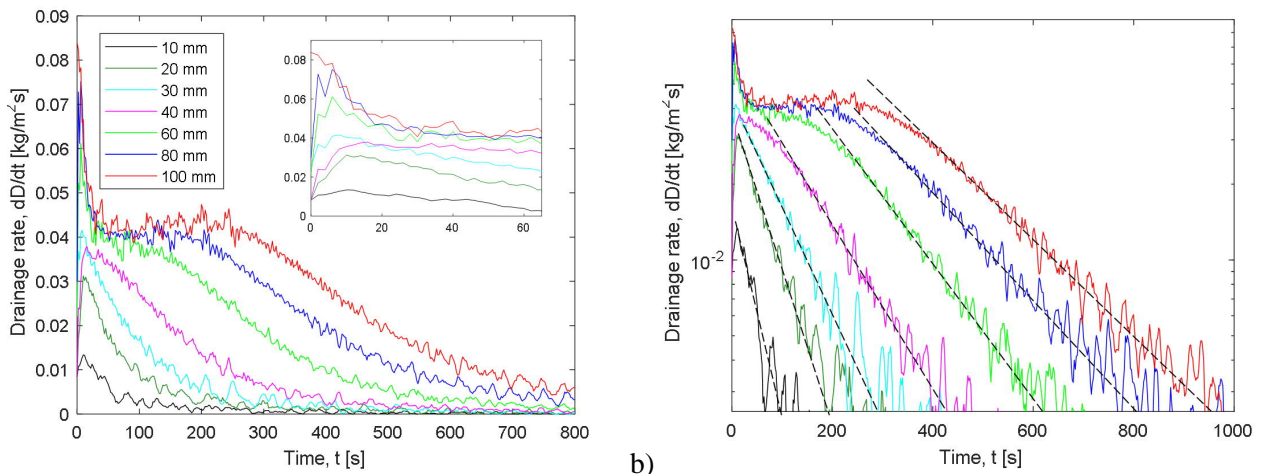
350 Figure 15 shows drainage as a function of time for pine fiber (trial points 11-17) with different mold
 351 heights. Birch and CTMP behaved qualitatively very similarly. We saw above that the time evolution
 352 of drainage could be given by Eq. (3) for a mold height of 40 mm with good accuracy. Although

353 drainage dynamics is more complicated for higher molds (see below), Eq. (3) can still be used for
 354 describing general drainage behavior. Figure 16 shows values of parameter T for the fit of Eq. (3) to
 355 the drainage data for different furnishes and mold heights. We can see from Figure 16 that the
 356 drainage process takes significantly longer (higher values of T) with increasing mold height and that
 357 the process is clearly faster for birch than for pine and CTMP. We currently have no explanation for
 358 this behavior. When the mold height is 40 mm or higher, T increases linearly with approximately the
 359 same slope with all three furnishes.



360

361 **Figure 16** Values of parameter T of Eq. (3) fitted to the drainage data for different furnishes and mold
 362 heights.



363

364 **Figure 17** Drainage rate for pine as a function of time for different mold heights in a) linear scale, b)
 365 log-lin scale. The inset in Figure a) shows the drainage rate during the first 65 seconds. With mold
 366 heights of 60, 80 and 100 mm, the drainage process consists of four phases: peak drainage rate,

367 constant drainage rate, transient phase, and exponentially decreasing drainage rate (see dashed
368 straight lines in b).

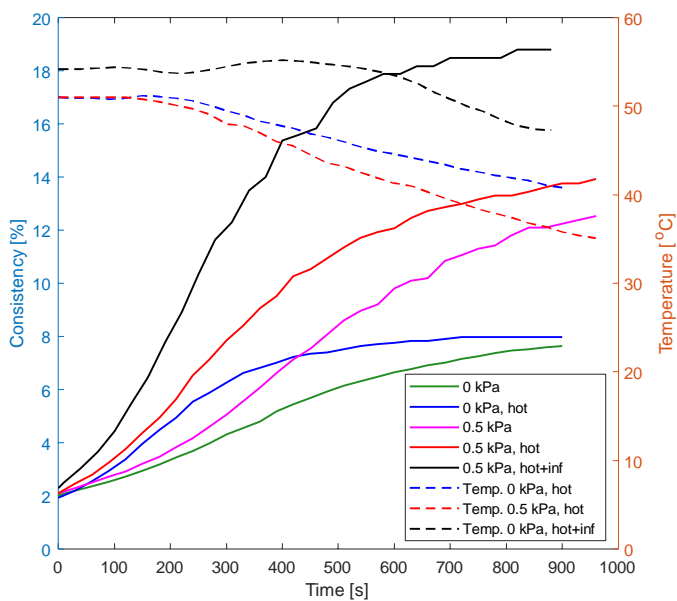
369 Figure 17 shows the drainage rate of pine as a function of time. We see from Figure 17 that initially
370 there is a short transient phase of the order of 10 seconds where the drainage rate increases from zero
371 to its maximum value. The drainage rate then starts to decrease exponentially with the 10-40 mm
372 mold heights. With mold heights of 60-100 mm, the behavior is more complex. After reaching its
373 peak value, the drainage rate drops rapidly during the next 20 seconds. Then, for a while, the drainage
374 rate is approximately constant; e.g. for the 100 mm mold this phase takes about 250 seconds. Finally,
375 the drainage rate starts to decrease exponentially. Koponen, Jäsberg, Lappalainen, and Kiiskinen
376 (2018) studied the initial drainage rate for 1.5% pine fiber foams in a closed container; at 65% and
377 70% air content, drainage rates were 0.072 kg/m²s and 0.057 kg/m²s, respectively. These values are
378 closely in line with our observed peak values for the 60-100 mm molds (see inset in Figure 17a).

379 **Table 3** Drainage experiments conducted with different vacuum levels (0–5 kPa). In trials 46–48 the
380 foam was initially heated to 50–55 °C. For trial 48, the foam was also heated with infrared radiation
381 during the drainage process. Initial consistency was ca. 2.2%. Left to right: trial point, furnish, mold
382 height, vacuum and heating (hot = initial heating of foam, inf. = initial heating of foam + infrared
383 heating), initial consistency, final consistency, amount of removed water, total shrinkage of the
384 sample, and shrinkage of the sample due to air leakage.

TP	Furnish	H_m [mm]	p [kPa]	ρ_i [%]	ρ_f [%]	w [%]	Δh [%]	Δh_{air} [%]
32	pine	80	0	2.1	8.2	76	25	3.2
33	pine	80	0.5	2.1	12.8	86	28	3.1
34	pine	80	1	2.1	14.5	86	28	2.3
35	pine	80	2	2.1	15.5	86	34	7.9
36	pine	80	3	2.1	17.6	88	38	9.8
37	pine	80	4	2.2	19.9	89	44	17
38	pine	80	5	2.2	22.0	90	50	25
39	birch	80	0	2.1	7.6	72	25	4.1
40	birch	80	0.5	2.3	12.9	83	28	3.8
41	birch	80	1	2.2	15.3	86	31	7.0
42	birch	80	2	2.2	16.3	86	35	9.6
43	birch	80	3	2.2	17.1	87	38	12
44	birch	80	4	2.1	16.3	87	40	16
45	birch	80	5	2.3	17.9	87	44	19
46	pine	80	0 (hot)	1.9	8.1	78	33	11
47	pine	80	0.5 (hot)	2.2	13.7	86	36	12
48	pine	80	0.5 (inf.)	2.3	19.1	90	35	10

385

386 We compared the drainage curves shown in Figure 17 with those obtained by solving the classical
 387 drainage equation for pure foams presented, for example, by Verbist et al. (1996) and Haffner et al.
 388 (2017). The qualitative behavior of drainage given by the model was similar to the measured
 389 behavior: with high mold heights the drainage rate peaked at the beginning of the process, and the
 390 drainage rate was then approximately constant before decreasing exponentially. With smaller molds
 391 the drainage rate started to decrease exponentially immediately. The time scale of drainage given by
 392 the model was, however, almost an order of magnitude longer than in the experiments. The time
 393 scales could be matched by multiplying the effective fluid viscosity by a free scaling parameter as
 394 was done by Haffner et al. (2017). The authors cannot, however, rigorously justify this method by the
 395 known properties of the system, thus it would be a pure numerical trick to circumvent the difference
 396 between the model and the experiments. New models are therefore evidently needed for quantitative
 397 description of the drainage of fiber-laden foams. For this purpose, we have offered all of the drainage
 398 measurements as open data (<https://zenodo.org/record/3585554>). We encourage readers to use these
 399 data as a basis for developing new models for the drainage of fiber-laden foams.



400

401 **Figure 18** Effect of vacuum level and heating on drainage of pine fiber foam. The foam temperature
 402 during drainage is also shown. Initial consistency is ca. 2.0% and the mold height is 80 mm.

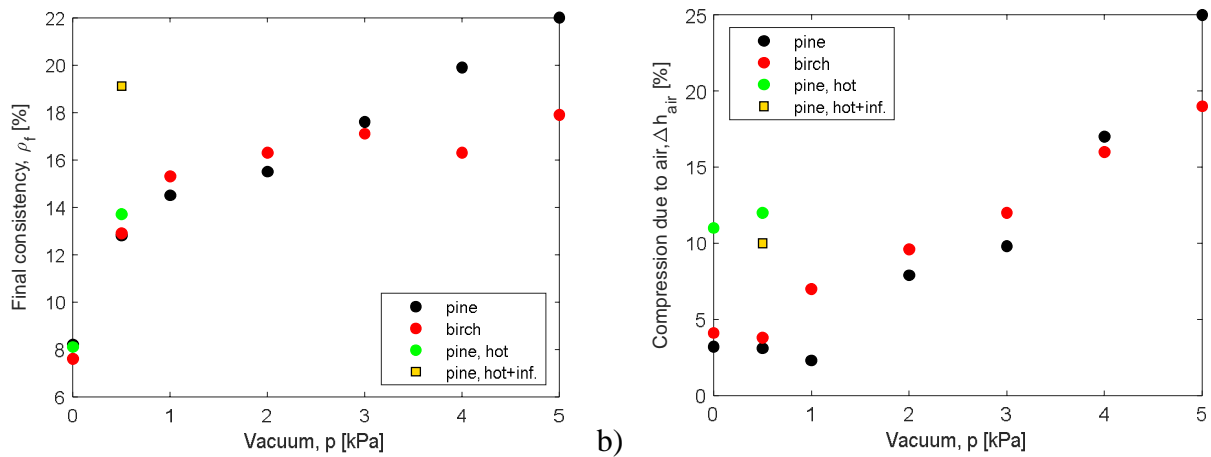
403 *Effect of low vacuum and fiber foam temperature on drainage*

404 Table 3 shows the trials points where the vacuum level was varied between 0-5 kPa. Most trials were
 405 performed at room temperature, but for trials 46, 47 and 48 the foam was initially heated to 50–55
 406 °C. At trial point 48 the foam was also heated during the drainage process with an infrared lamp.

407 Figure 18 shows the time evolution of consistency for pine for different vacuum and heating
 408 conditions. Due to decreasing water viscosity, heating increases the drainage rate considerably both
 409 with and without 0.5 kPa vacuum.

410 Figure 19a shows the effect of vacuum and heating on the final consistency. We see in Figure 19a
 411 that consistency is clearly improved when vacuum is used, but the benefit decreases with increasing
 412 vacuum level. With birch, final consistency starts to saturate already with a vacuum of 3 kPa. Heating
 413 the foam is seen to have only a minor effect on the final consistency unless the foam is also heated
 414 during the drainage process. In that case, the final consistency is significantly increased to the same
 415 level as with the highest vacuums. Notably, the consistencies obtained with the highest vacuum are
 416 similar to those seen in paper machines after the forming board (Koponen, Haavisto, Liukkonen, &
 417 Salmela, 2016).

418 As discussed above, the samples compress during drainage by at least as much as the volume of
 419 drained water. In addition to this, some extra compression takes place due to leakage of air out of the
 420 sample. Figure 19b shows the effect of vacuum and heating on the compression of the sample due to
 421 leakage of air. We can see in Figure 19b that Δh_{air} is similar with and without a 0.5 kPa vacuum. With
 422 higher vacuum levels compression increases, reaching about 20% with the highest vacuum of 5 kPa.
 423 We also see in Figure 19b that heating the foam increases compression significantly.



424 a) b)
 425 **Figure 19** Effect of vacuum and heating on a) final consistency and b) compression of the sample
 426 due to leakage of air. Initial consistency ca. 2.2% and mold height 80 mm.

427 Conclusions

428 Foam forming is a promising method for making lightweight lignocellulosic fibrous materials. Unlike
 429 water, the bubbles in foam support the fibrous structure during manufacturing, enabling the formation

430 of highly porous structures. As mechanical pressure cannot be used, it is important to remove as much
431 water as possible from the fibrous structures by drainage before thermal drying. Timofeev et al.
432 (2016) have shown that shrinkage of the structures during thermal drying can be eliminated by
433 choosing the right drying conditions. Minimizing the shrinkage of the sample during drainage is thus
434 critical for the successful manufacture of LLMF structures.

435 In addition to analyzing free drainage, we studied the effect of vacuum and heating of foam on
436 drainage. We found that by the end of drainage a stationary horizontal moisture profile is developed
437 that is similar to that of pure foams. Rising initial consistency increased the final consistency of the
438 foam until drainage ceased. Increasing the mold height increased the final consistency considerably.
439 Without application of vacuum and heating, sample shrinkage during drainage was only slightly
440 higher than the volume of the drained water. Drainage rate and final consistency increased clearly
441 with increasing vacuum, but at the same time sample shrinkage increased considerably. The best
442 compromise was obtained with a vacuum of 0.5 kPa, which increased the final consistency by 60%
443 without extra shrinkage. Using warm foam and heating the foam during drainage increased the final
444 consistency considerably, but this also led to significant shrinkage of the sample.

445 Future studies should investigate possibilities for strengthening the fibrous structures to allow higher
446 vacuums and higher foam temperatures. One option is to add small amounts of cellulose nanofibrils
447 to the structure (Cervin et al., 2013). The drainage process can also possibly be further optimized by
448 using increasing vacuum as a function of time. This could minimize sample shrinkage during
449 drainage.

450 **Acknowledgements**

451 This work was conducted as part of the Future Fibre Products 2020 (FFP2020) project, which is
452 funded by the European Regional Development Fund (grant number A73089, A73092), VTT
453 Technical Research Centre of Finland Ltd., and 32 industrial partners.

454 Open data: <https://zenodo.org/record/3585554>

455 **Declaration on conflict of interest:** The authors declare no conflict of interest.

456 **References**

457 Alimadadi, M., & Uesaka, T. (2016). 3D-oriented fiber networks made by foam forming. *Cellulose*,
458 23(1), 661–671. <https://doi.org/10.1007/s10570-015-0811-z>

- 459 Arjmandi-Tash, O., Kovalchuk, N., Trybala, A., & Starov, V. (2015). Foam drainage placed on a
460 porous substrate. *Soft Matter*, *11*(18), 3643–3652. <https://doi.org/10.1039/c5sm00377f>
- 461 Burke, S., Möbius, M., Hjelt, T., & Hutzler, S. (2019). Properties of lightweight fibrous structures
462 made by a novel foam forming technique. *Cellulose*, *26*(4), 2529–2539.
463 <https://doi.org/10.1007/s10570-018-2205-5>
- 464 Cervin, N., Andersson, L., Ng, J., Olin, P., Bergström, L., & Wågberg, L. (2013). Lightweight and
465 strong cellulose materials made from aqueous foams stabilized by nanofibrillated cellulose.
466 *Biomacromolecules*, *14*(2), 503–511. <https://doi.org/10.1021/bm301755u>
- 467 Cervin, N., Aulin, C., Larsson, P., & Wågberg, L. (2012). Ultra porous nanocellulose aerogels as
468 separation medium for mixtures of oil/water liquids. *Cellulose*, *19*(2), 401–410.
469 <https://doi.org/10.1007/s10570-011-9629-5>
- 470 Debeleac, C., Nechita, P., & Nastac, S. (2019). Computational investigations on soundproof
471 applications of foam-formed cellulose materials. *Polymers*, *11*(7), 1–20.
472 <https://doi.org/10.3390/polym11071223>
- 473 Haffner, B., Dunne, F., Burke, S., & Hutzler, S. (2017). Ageing of fibre-laden aqueous foams.
474 *Cellulose*, *24*(1), 231–239. <https://doi.org/10.1007/s10570-016-1100-1>
- 475 Härkäsalmi, T., Lehmonen, J., Itälä, J., Peralta, C., Siljander, S., & Ketoja, J. (2017). Design-driven
476 integrated development of technical and perceptual qualities in foam-formed cellulose fibre
477 materials. *Cellulose*, *24*(11), 5053–5068. <https://doi.org/10.1007/s10570-017-1484-6>
- 478 Hertzendorf, M., Moshy, R., & Seltzer, E. (1970). Foam drying in the food industry. *C R C Critical*
479 *Reviews in Food Technology*, 25–70. <https://doi.org/10.1080/10408397009527099>
- 480 Huber, T., Müssig, J., Curnow, O., Pang, S., Bickerton, S., & Staiger, M. (2012). A critical review
481 of all-cellulose composites. *Journal of Materials Science*, *47*(3), 1171–1186.
482 <https://doi.org/10.1007/s10853-011-5774-3>
- 483 Josset, S., Hansen, L., Orsolini, P., Griffa, M., Kuzior, O., Weisse, B., Zimmermann, T., & Geiger,
484 T. (2017). Microfibrillated cellulose foams obtained by a straightforward freeze–thawing–
485 drying procedure. *Cellulose*, *24*(9), 3825–3842. <https://doi.org/10.1007/s10570-017-1377-8>
- 486 Koehler, S., Hilgenfeldt, S., & Stone, H. (2000). *A generalized view of foam drainage: experiment*
487 *and theory*, *Langmuir* *16*(15), 6327–6341. <https://doi.org/10.1021/la9913147>

- 488 Koponen, A., Haavisto, S., Liukkonen, J., & Salmela, J. (2016). The flow resistance of fiber sheet
489 during initial dewatering. *Drying Technology*, *34*(12), 1521-1533.
490 <https://doi.org/10.1080/07373937.2015.1132427>
- 491 Koponen, A., Jäsberg, A., Lappalainen, T., & Kiiskinen, H. (2018). The effect of in-line generation
492 of foam on the foam quality and the sheet formation in foam forming. *Nordic Pulp & Paper*
493 *Research Journal*. *33*(3), 482-495. <https://doi.org/10.1515/npprj-2018-3051>
- 494 Koponen, Antti, Torvinen, K., Jäsberg, A., & Kiiskinen, H. (2016). Foam forming of long fibers.
495 *Nordic Pulp & Paper Research Journal*, *31*(2), 239–247. [https://doi.org/10.3183/npprj-2016-](https://doi.org/10.3183/npprj-2016-31-02-p239-247)
496 [31-02-p239-247](https://doi.org/10.3183/npprj-2016-31-02-p239-247)
- 497 Korehei, R., Jahangiri, P., Nikbakht, A., Martinez, M., & Olson, J. (2016). Effects of drying
498 strategies and microfibrillated cellulose fiber content on the properties of foam-formed paper.
499 *Journal of Wood Chemistry and Technology*, *36*(4), 235–249.
500 <https://doi.org/10.1080/02773813.2015.1116012>
- 501 Koursari, N., Arjmandi-Tash, O., Johnson, P., Trybala, A., & Starov, V. (2019). Foam drainage
502 placed on a thin porous layer. *Soft Matter*, *15*(26), 5331–5344.
503 <https://doi.org/10.1039/c8sm02559b>
- 504 Kowalczyk, P., & Drzymala, J. (2016). Physical meaning of the Sauter mean diameter of spherical
505 particulate matter. *Particulate Science and Technology*, *34*(6), 645–647.
506 <https://doi.org/10.1080/02726351.2015.1099582>
- 507 Kowalski, S. (Ed.). (2007). *Drying of Porous Materials*. Springer.
- 508 Kruglyakov, P., Elaneva, S., Vilkova, N., & Karakashev, S. (2010). Investigation of foam drainage
509 using foam pressure drop technique. *Colloids and Surfaces A: Physicochemical and*
510 *Engineering Aspects*, *354*(1–3), 291–297. <https://doi.org/10.1016/j.colsurfa.2009.06.014>
- 511 Kruglyakov, P., Karakashev, S., Nguyen, A., & Vilkova, N. (2008). Foam drainage. *Current*
512 *Opinion in Colloid and Interface Science*, *13*(3), 163–170.
513 <https://doi.org/10.1016/j.cocis.2007.11.003>
- 514 Kudra, T., & Ratti, C. (2006). Foam-mat drying: Energy and cost analyses. *Canadian Biosystems*
515 *Engineering / Le Genie Des Biosystems Au Canada*, *48*, 27–32.
- 516 Kushner, L., Duncan, B., & Hoffman, J. (1952). A viscometric study of the micelles of sodium

- 517 dodecyl sulfate in dilute solutions. *Journal of Research of the National Bureau of Standards*,
518 49(2), 85–90.
- 519 Lappalainen T., & Lehmonen J. (2012). Determinations of bubble size distribution of foam-fibre
520 mixture using circular hough transform. *Nordic Pulp and Paper Research Journal*, 27(05),
521 930–939. <https://doi.org/10.3183/NPPRJ-2012-27-05-p930-939>
- 522 Lehmonen, J., Retulainen, E., Paltakari, J., Kinnunen-Raudaskoski, K., & Koponen, A. (2020).
523 Dewatering of foam-laid and water-laid structures and the formed web properties. *Cellulose*,
524 27(3): 1127–1146. <https://doi.org/10.1007/s10570-019-02842-x>
- 525 Li, S., Xiang, W., Järvinen, M., Lappalainen, T., Salminen, K., & Rojas, O. J. (2016). Interfacial
526 stabilization of fiber-laden foams with carboxymethylated lignin toward strong nonwoven
527 networks. *ACS Applied Materials and Interfaces*, 8(30), 19827–19835.
528 <https://doi.org/10.1021/acsami.6b06418>
- 529 Lyons, D., & Vollers, C. (1971). The drying of fibrous materials. *Textile Research Journal*, 41(8),
530 661–668.
- 531 Mira, I., Andersson, M., Boge, L., Blute, I., Carlsson, G., Salminen, K., Lappalainen, T., &
532 Kinnunen, K. (2014). Foam forming revisited Part I. Foaming behaviour of fibre-surfactant
533 systems. *Nordic Pulp and Paper Research Journal*, 29(04), 679–689.
534 <https://doi.org/10.3183/NPPRJ-2014-29-04-p679-689>
- 535 Miralles, V., Selva, B., Cantat, I., & Jullien, M. (2014). Foam drainage control using
536 thermocapillary stress in a two-dimensional microchamber. *Physical Review Letters*, 112(23),
537 1–5. <https://doi.org/10.1103/PhysRevLett.112.238302>
- 538 Nechita, P., & Năstac, S. (2018). Foam-formed cellulose composite materials with potential
539 applications in sound insulation. *Journal of Composite Materials*, 52(6), 747–754.
540 <https://doi.org/10.1177/0021998317714639>
- 541 Papara, M., Zabulis, X., & Karapantsios, T. (2009). Container effects on the free drainage of wet
542 foams. *Chemical Engineering Science*, 64(7), 1404–1415.
543 <https://doi.org/10.1016/j.ces.2008.11.021>
- 544 Pöhler, T., Jetsu, P., Fougerón, A., & Barraud, V. (2017). Use of papermaking pulps in foam-
545 formed thermal insulation materials. *Nordic Pulp and Paper Research Journal*, 32(3), 367–

- 546 374. <https://doi.org/10.3183/npprj-2017-32-03-p367-374>
- 547 Poranen, J., Kiiskinen, H., Salmela, J., Asikainen, J., Keränen, J., & Paakkonen, E. (2013). Break-
548 through in papermaking resource efficiency with foam forming. *Proceedings of TAPPI*
549 *PaperCon, Atlanta, GA, USA*, 807–814.
- 550 Punton, V. (1975a). Fibre distribution in foam and foam-laid paper. *Int. Paper Physics Conf.*, 135–
551 139.
- 552 Punton, V. (1975b). The use of an aqueous foam as a fibre-suspending medium in quality
553 papermaking. *Proceedings of a Symposium Organized by the Society of the Chemical Industry.*
554 *Colloid and Surface Chemistry Group*, 179–194. Brunel University.
- 555 Saint-Jalmes, A. (2006). Physical chemistry in foam drainage and coarsening. *Soft Matter*, 2(10),
556 836. <https://doi.org/10.1039/b606780h>
- 557 Sangamithra, A., Venkatachalam, S., John, S., & Kuppaswamy, K. (2015). Foam mat drying of
558 food materials: a review. *Journal of Food Processing and Preservation*, 39(6), 3165–3174.
559 <https://doi.org/10.1111/jfpp.12421>
- 560 Satyanarayana, K., Arizaga, G., & Wypych, F. (2009). Biodegradable composites based on
561 lignocellulosic fibers - an overview. *Progress in Polymer Science (Oxford)*, 34(9), 982–1021.
562 <https://doi.org/10.1016/j.progpolymsci.2008.12.002>
- 563 Sehaqui, H., Zhou, Q., Ikkala, O., & Berglund, L. (2011). Strong and tough cellulose nanopaper
564 with high specific surface area and porosity. *Biomacromolecules*, 12(10), 3638–3644.
565 <https://doi.org/10.1021/bm2008907>
- 566 Siljander, S., Keinänen, P., Ivanova, A., Lehmonen, J., Tuukkanen, S., Kanerva, M., & Björkqvist,
567 T. (2019). Conductive cellulose based foam formed 3D shapes—from innovation to designed
568 prototype. *Materials*, 12(3), 1–12. <https://doi.org/10.3390/ma12030430>
- 569 Smith, M., & Punton, V. (1975). Foam can improve formation. *Pulp & Paper Canada*, 76(1), 55–
570 58.
- 571 Smith, M., Punton, V., & Rixson, A. (1974). The structure and properties of paper formed by a
572 foaming process. *Tappi Journal*, 57(1), 107-111.
- 573 Stenström, S. (2019). Drying of paper: A review 2000–2018. *Drying Technology*.

574 <https://doi.org/10.1080/07373937.2019.1596949>

575 Stevenson, P. (2006). Dimensional analysis of foam drainage. *Chemical Engineering Science*,
576 *61*(14), 4503–4510. <https://doi.org/10.1016/j.ces.2006.02.026>

577 Timofeev, O., Jetsu, P., Kiiskinen, H., & Keränen, J. (2016). Drying of foam-formed mats from
578 virgin pine fibers. *Drying Technology*, *34*(10), 1210–1218.
579 <https://doi.org/10.1080/07373937.2015.1103254>

580 Verbist, G., Weaire, D., & Kraynik, A. (1996). The foam drainage equation. *Journal of Physics*
581 *Condensed Matter*, *8*(21), 3715–3731. <https://doi.org/10.1088/0953-8984/8/21/002>

582 Wege, H., Kim, S., Paunov, V., Zhong, Q., & Velev, O. (2008). Long-term stabilization of foams
583 and emulsions with in-situ formed microparticles from hydrophobic cellulose. *Langmuir*,
584 *24*(17), 9245–9253. <https://doi.org/10.1021/la801634j>

585 Xu, P., Sasmito, A., & Mujumdar, A. (2019). *Heat and Mass Transfer in Drying of Porous Media*.
586 CRC Press.

587

588

589

590

591

592